A High-Temperature Superconducting Helmholtz Probe for Microscopy at 9.4 T

S.E. Hurlston,[1] W.W. Brey,[2] S.A. Suddarth,[1] and G.A. Johnson[1]

The design and operation of a high-temperature superconducting (HTS) probe for magnetic resonance microscopy (MRM) at 400 MHz are presented. The design of the probe includes a Helmholtz coil configuration and a stable open-cycle cooling mechanism. Characterization of coil operating parameters is presented to demonstrate the suitability of cryo-cooled coils for MRM. Specifically, the performance of the probe is evaluated by comparison of signal-to-noise (SNR) performance with that of a copper Helmholtz pair, analysis of B_1 field homogeneity, and quantification of thermal stability. Images are presented to demonstrate the SNR advantage of the probe for typical MRM applications. Magn Reson Med 41:1032–1038, 1999.

Key words: MR microscopy; HTS probe; SNR

The resolution limit in magnetic resonance microscopy (MRM) is affected by a number of factors, the most significant being the signal-to-noise ratio (SNR) available as voxel size is decreased. One barrier to attaining SNR at high resolution is the noise introduced by the receiver coil. As the size of a sample decreases, the thermal noise of the receiver coil starts to represent a greater proportion of the total system noise, and eventually a point is reached where the coil rather than the sample determines the SNR at the preamplifier (1,2). In an effort to limit receiver coil noise for both small sample and low magnetic field applications, a number of investigators have reported the use of high temperature superconducting (HTS) materials in the construction of low-noise radiofrequency (RF) coils (2–6).

The work presented by Black et al (7) demonstrated the use of a 300 MHz HTS resonator fabricated from $Y_1Ba_2Cu_3O_7$ (YBCO) with a field of view of approximately 1 cm, operating at a temperature of 10 K. The SNR gain from using the HTS coil was ~10× when compared with a single copper coil of identical dimensions. Later work (8) utilized the same HTS coil configuration to produce an improvement of 4× in SNR over a solenoid coil. In another investigation, Miller et al (5) reported an SNR gain of 10× for a $Tl_2Ba_2CaCu_2O_8$ (TBCCO) resonator used in sodium imaging at 32 MHz. Again, the HTS resonator was used in a surface coil configuration, and the comparison room temperature copper coil was of similar dimensions and magnetic field pattern.

Recently, HTS NMR spectroscopy probes utilizing YBCO coils have been reported to produce sensitivity improvement by a factor of 4–5 over conventional probes (9). The probes have been operated in both closed- and open-cycle cooling configurations. The sample is contained within a 5-mm-diameter tube that runs through the center of a Helmholtz coil pair. The pair of HTS coils is inductively coupled both to one another and to a copper pick-up loop, which acts as a matching interface to the T/R switch. The cooling approach involves a single-walled dewar that allows the coil to be located as close to the sample as possible. The coil substrates are mounted to a copper coldhead cooled by a helium gas stream (10).

We report the implementation of a probe based on the approach of Kotsubo, described above (9,10), modified to be used for MRM at 9.4 T. A prior generation of this probe has been presented elsewhere (11). The probe accommodates a cylindrical sample tube of 5-mm outer diameter. The bore diameter is appropriate for imaging tissue samples of interest in our MRM studies. The use of a Helmholtz pair allows for a more nearly uniform RF field than the single-coil HTS designs employed in previous investigations. The performance of the HTS probe was compared with a well-characterized copper Helmholtz coil (12) of similar dimensions. The parameters used for comparison included quality factor (Q) under typical coil loading conditions, SNR for a water phantom and an in vitro mouse kidney sample, and RF uniformity. As a means for evaluating each coil, we present a model for predicting SNR from easily measured or calculated quantities. This model represents a synthesis of theory presented previously (3,13–15) and serves to emphasize the relevant parameters used to gauge the experimental SNR performance of a cooled coil.

MATERIALS AND METHODS

Probe and Coil Design

A detailed depiction of the design of the YBCO coils is indicated in Fig. 1a. The coil resonance was achieved through the use of interdigital capacitance, as described elsewhere (4). Breaking each coil with two interdigital capacitors results in a low residual electric field. These coils are positioned at the top of the open-cycle, metal-walled probe shown in Fig. 1b. The operation of the HTS probe can be described by discussing the features highlighted in this figure. The coils are deposited on sapphire substrates that directly contact a copper coldhead, cooling the coils by thermal conduction. The coldhead in turn is cooled to the typical operating temperature of 20 K by a stream of cold helium gas. The thermal stability of the coils was regulated by a temperature controller (Conductus, Sunnyvale, CA) with a ruthenium oxide sensor positioned at the coldhead. During transmit, power dissipated as heat did not produce any noticeable change in the thermal regulation of the probe, so that the temperature reading on

[1]Center for *In Vivo* Microscopy, Duke University Medical Center, Durham, North Carolina.

[2]Conductus, Inc., Sunnyvale, California.

Grant sponsor: NIH NCRR; Grant number: P41 RRO5959; Grant sponsor: NSF; Grant number: CDR-8622201; Grant sponsor: NIH; Grant number: 2R44RR09244; Grant sponsor: ARPA; Grant number: DAMD17-94-J-4496.

Correspondence to: Elaine G. Fitzsimons, Center for *In Vivo* Microscopy, Box 3302 DUMC, Durham, NC 27710. E-mail: egf@orion.mc.duke.edu

Received 21 July 1998; revised 30 November 1998; accepted 5 January 1999.

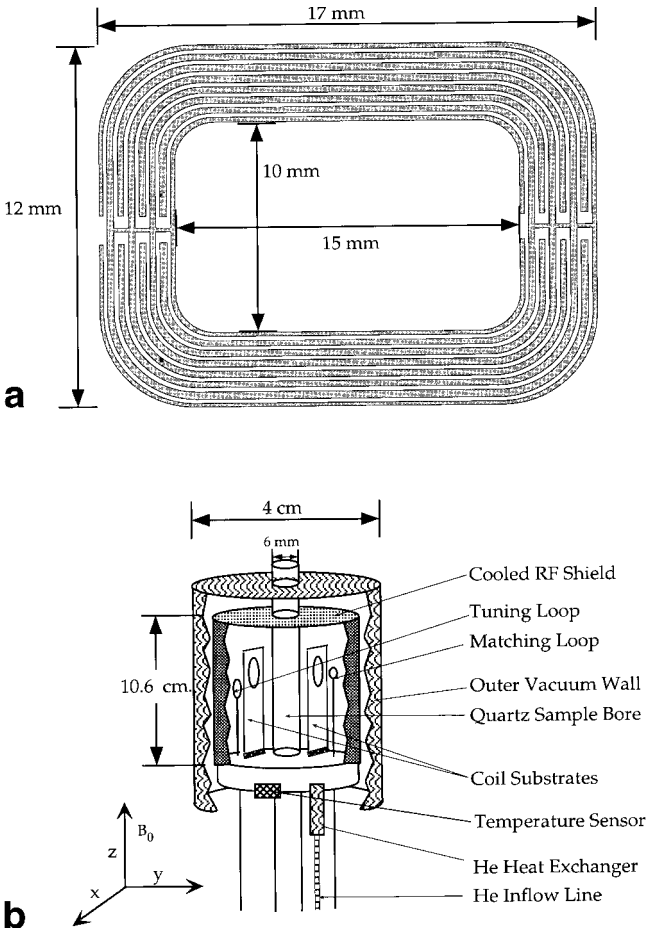

FIG. 1. **a:** Schematic of coils positioned at the top of the probe in b. **b:** Schematic of HTS probe highlighting several important technical features.

the controller remained within ±0.05 K of the set point. Tuning and matching were achieved through the use of two loops of copper wire: a tuning loop that provided an inductive shift for the resonant frequency, and a matching loop that provided the electrical connection to the T/R switch and the preamplifier. Using a pair of micrometers, the vertical position of both loops with respect to the coils could be controlled from outside of the bore of the magnet while the probe was in operation. The rigid cable extending from the loop to these micrometers is vacuum-isolated by a system of o-rings. The sample was positioned inside a quartz sample bore, which was thermally isolated from the coils by a vacuum on the order of 30 mTorr inside the metal-walled structure. While the vacuum provided significant thermal isolation, some cooling of the inner bore tube occurred as the result of radiative heat exchange with the sapphire coil substrates. This problem was addressed by circulating dry, room temperature air through the bore tube, ensuring a stable sample temperature.

Microscopic Imaging System and Experimental Imaging Parameters

The probe was inserted into a vertical bore 9.4 T imaging system with an S-50 Microstar gradient set (Bruker Instruments, Fremont, CA). The probe was designed to have the geometric center of the coil pair located at gradient center when loaded from the bottom of the magnet. Samples could be placed into a sample holder and inserted into the probe from the top of the magnet. The imaging system is operated from an Omega CSI console (Bruker Instruments). The noise figure of this system, measured using the hot/cold resistor method, is about 2 dB, which is equivalent to a noise temperature of ~170 K. A custom low-noise GaAs-FET preamplifier (Berkshire Technologies, Emeryville, CA) was added to the system for all experiments. The design of this preamplifier reduces the need for bandwidth broadening with the high *Q* HTS resonators by providing a flat gain over a wide range of input impedance values (16). A passive protection circuit has also been added to the system for use with the 5-mm HTS probe. With the preamplifier held at a physical temperature of 77 K, the system noise temperature, including the T/R switch, was reduced to 50 K. This system configuration was used for the HTS probe during both phantom and in vitro experiments and for the copper probe during phantom experiments only. For operation with the copper Helmholtz probe and in vitro sample, a second protection circuit was substituted due to the need for additional transmit power. For this particular experiment, the total system noise temperature was measured to be 90 K, which was still substantially less than the 300 K physical temperature of the copper probe.

SNR measurements were made from images of a mouse kidney and slice-selective images from a small water sample. These two samples were chosen to ensure the fairest possible comparison in light of the effect of sensitivity, sample loading, susceptibility, and eddy currents on measurement of SNR. For in vitro measurement of SNR, two freshly excised kidney samples were used to ensure that no differential desiccation or postmortem changes in T_1/T_2 had occurred between experiments. Immediately following anesthesia and opening of the abdomen, the renal vein was ligated to utilize the innate contrast provided by the blood (Oliverio, unpublished work). The kidneys were placed in a 5-mm glass NMR tube and surrounded by the lubricant Fomblin (Ausimont USA, Morristown, NJ), a branched perfluropolyether that does not add extraneous signal to ^{1}H images. This surrounding fluid minimizes the susceptibility artifact at the surface of the specimen. The kidneys were then imaged, the first using a room temperature Helmholtz coil, and the second with the 5-mm HTS probe, with identical sequence parameters: a three-dimensional (3D) spin-echo sequence with a TR of 500 msec, TE of 20 msec, number of excitations 1, and a 50 kHz bandwidth. The image matrix was 512 × 256 × 32 over a field of view (FOV) of 8.6 × 4.3 × 4.3 mm, yielding an in-plane resolution of 17 μm (voxel volume = 3.8×10^{-5} mm^3). Both coils were tuned to a resonant frequency of 400.2 MHz and matched to 50 Ω immediately prior to imaging.

To evaluate the SNR gain of the HTS probe, calculated intensity images that mapped the SNR across a single slice were generated for the kidney data. Comparison slices were taken from approximately the same plane in both samples. The SNR was calculated by the method described by Edelstein et al (17) using a signal region of 4 × 4 pixels

and a noise region of 50 × 50 pixels to ensure an accuracy within 10%. The SNR was calculated across the entire image, and the maximum, minimum, and mean SNRs for each image were extracted.

Using a homogeneous water sample, axial slice-selective images were taken with the two probes while stepping through a range of transmit attenuation values to maximize the signal across the greatest proportion of the sample. For this comparison, the same passive protection circuit was used for both coils. Resistance in this protection circuit attenuated the RF pulse power so that the duration of the RF pulse needed to be lengthened for the copper probe (4-msec pulse compared with a 2-msec pulse) to attain the maximum signal point. The experimental parameters included a TR of 200 msec, a TE of 20 msec, a slice thickness of 2 mm, an image matrix of 512 × 256, an imaging bandwidth of 50 kHz, and an FOV of 8 mm^2. For both coils, the water sample was placed in a 5-mm NMR glass tube, and the axis of the tube was aligned with the z-axis of the magnet and probe. The SNR across these images was calculated using the method described above. Homogeneity was determined based on a histogram of the SNR values within these images. Sagittal slice-selective images were also acquired using similar imaging parameters, with the exception of a 20 mm^2 FOV and a 0.2-mm slice thickness for the HTS coil. The high sensitivity of the HTS probe allowed the use of the thinner slice to attain a more precise measure of the B_1 homogeneity in the center of the probe.

Because the properties of the RF coils are dependent on temperature, stability of the coil was critical to establish the suitability for high-resolution microscopic imaging. The resonant frequency and the Q of the probe were measured as the regulated temperature was varied. Data were also acquired on the variation of temperature over the course of operation.

Q Measurements and Comparison With Theory

To validate the experimental measure of SNR, we present a theoretical model that derives the relationship between SNR, operating temperature, noise temperature, Q, and the B_1 per unit current for each probe configuration. This model is centered on the equations first presented by Jerosch-Herold and Kirschman (13), which allow separate comparison of signal and noise for matched coils. Their model is tailored to our particular comparison, and parameter values are derived from measurable quantities whenever possible.

The model calculates the B_1 field for each coil configuration using the Biot-Savart law. The field of the copper Helmholtz resonator at the center of the coil pair was derived by summing the field of the individual coils (12):

$$\frac{B_1}{I} = \frac{\mu_0 a^2}{\left(\left(\frac{s}{2}\right)^2 + a^2\right)^{3/2}}, \qquad [1]$$

where a is the radius of the coil in meters and s is the separation distance between the coils. Similarly, the B_1 for both of the rectangular-coil Helmholtz HTS resonators was derived:

$$\frac{B_1}{I} = \frac{4\mu_0 l_1 l_2}{\pi\sqrt{l_1^2 + l_2^2 + s^2}}\left(\frac{1}{l_1^2 + s^2} + \frac{1}{l_2^2 + s^2}\right), \qquad [2]$$

where l_1 and l_2 are the length of the top and side rungs of the coil in meters, and s is the separation distance between the coils. For the copper Helmholtz probe, the value for the inductance, L, was determined by direct measurement of the coil's capacitance, C, and resonant frequency, f_0, and from the equation:

$$2\pi f_0 = \frac{1}{\sqrt{LC}}, \qquad [3]$$

assuming a coil with a reasonable Q. Because direct measurement is complicated by the cooling process, the inductance of the HTS coils was approximated using a method of moments calculation provided in the IE3D software package (Zeland Software, Fremont, CA).

Using the above formulas for inductance, the resistance of both the sample and the coil could be derived from the unloaded and loaded Q values measured for each coil. Q values were measured using a 4195A Spectrum/Network analyzer (Hewlett Packard, Palo Alto, CA) calibrated to the frequency range of interest and set to measure return loss (4). All Q measurements were made with the coil of interest matched to 50 Ω. Note that the term ''unloaded'' is used to imply that the sample is not present when the measurement is made. The value of the Q was then doubled for the purposes of calculation to reflect the unmatched Q. The resistance of the coil could be derived from this adjusted measurement of the unloaded Q and the well-known formula:

$$R_{\text{coil}} = \frac{2\pi f_o L}{Q_{\text{unloaded}}}, \qquad [4]$$

where f_o is the resonant frequency of the coil. The resistance of the sample was calculated by determining the Q of the sample and then inserting this value into Eq. [4]:

$$R_{\text{sample}} = 2\pi f_o L\left(\frac{1}{Q_{\text{loaded}}} - \frac{1}{Q_{\text{unloaded}}}\right), \qquad [5]$$

where Q_{loaded} denotes the Q in the presence of the sample, and the inductance added by the sample is neglected. The relative signal voltage, V_s, could then be calculated by combining Eqs. [1], [4], and [5] for the copper coils, and Eqs. [2], [4], and [5] for the HTS coils (13,18,19):

$$V_s \propto \frac{B_1}{I\sqrt{R_{\text{coil}} + R_{\text{sample}}}}. \qquad [6]$$

To calculate the noise voltage for each coil, the system noise parameters were determined experimentally using a hot-cold resistor measurement, as briefly described above. Next, the resistor termination for the preamplifier was replaced with the HTS probe to determine its operating

noise temperature, which is generally higher than the physical temperature of the probe. For the purpose of SNR measurements, this effective operating temperature represents a combination of the temperature of the coil and sample, as follows (13):

$$T_{\text{probe}} = \frac{T_{\text{coil}}R_{\text{coil}} + T_{\text{sample}}R_{\text{sample}}}{R_{\text{coil}} + R_{\text{sample}}}, \quad [7]$$

where T_{coil} represents the measured noise temperature of the coil, T_{sample} represents the physical temperature of the sample, and R_{coil} and R_{sample} are the resistance values described above. The relative noise voltage, V_n, of each coil could then be calculated, based on the fundamental Johnson thermal noise equation:

$$V_n \propto \sqrt{T_{\text{probe}} + T_{\text{system}}} \quad [8]$$

where the system noise figure has been converted to the value T_{system}. Finally, the projected system SNR can be calculated by dividing Eq. [6] by Eq. [8]. By dividing the numbers for the SNR of the HTS coil and the SNR of the copper coil, respectively, a gain index was calculated as a numerical measure of the SNR advantage achieved by using the HTS coil.

RESULTS AND DISCUSSION

Evaluation of SNR

Table 1 summarizes the physical measurements relevant to the prediction of SNR for the two coils in this study. Note that the physical dimensions listed in this table correspond to the inner diameter and separation distance for the copper probe, and the height, width, and separation distance, respectively, for the HTS Helmholtz pair. While the comparison coil is not identical to the HTS coils, the inner diameter, where most of the current travels (12), is roughly equal to the mean diameter of the HTS coils measured at the center of each 2-mm trace. The current flow in the HTS coil is more uniform than that of the copper coil due to the use of interdigital capacitance. Using these assumptions, the value of B_1 per unit current is ~1 G/A for both coils. The loaded, matched Q values are reported for the two samples that were used in measurements of SNR from both coils. Since the calculated values for the inductance of the coils in each probe are both ~30 nH, the factor of ~100 increase in Q can largely be attributed to the reduced resistance of the HTS resonators. Inserting the values from Table 1 into Eqs. [4]–[8] above, the SNR advantage of the HTS coil over the solenoid was estimated to be greater by a factor of 12 for the mouse kidney sample and a factor of 14 for the water phantom. A simple comparison of the ratio $\sqrt{Q/T}$ (7) yields a substantial overestimate of the SNR gain with a prediction of a 24-fold improvement. Inclusion of sample loading effects and system noise temperature yields a more accurate estimate of the SNR advantage in a cooled coil system (13).

Table 1
Coil Parameters for Comparison Study

Parameter	Value for HTS probe	Value for copper Helmholtz
Dimensions	11 × 16 × 9 mm ($w_1 \times w_2 \times s$)	13 × 9 mm (D × s)
Unloaded matched Q	18,000	160
Loaded Q (mouse kidney)	12,000	140
Loaded Q (water phantom)	16,000	150
Coil noise temperature	77 K	300 K
Calculated B_1/A	1.03 G/A	1.10 G/A
Calculated inductance, L	28 nH	27 nH

Images demonstrating the SNR increase attained with the HTS probe and the mouse kidney sample are shown in Fig. 2a and b. Note that Fig. 2a corresponds to a single slice of the 3D data set for the copper Helmholtz coil, while Fig. 2b corresponds to a comparable slice in the HTS data set. The images in Fig. 2a and b show a substantial difference in the observed SNR, as defined by a grainier appearance of the copper Helmholtz image and by the lack of contrast and definition throughout the kidney. In contrast, the HTS image shows a clear distinction between the inner medulla and renal pelvis and the cortex and outer medulla regions (20). In addition, very fine inner structures, such as the collecting tubules indicated by the striations in the inner medulla and renal pelvis, are visible in the HTS image. Numerical analysis of SNR within these images is difficult due to the effect of contrast, B_1 homogeneity, and anatomical registration on the measurement. The differential between the size of the two kidneys also complicates the comparison of SNR by anatomical registration, but should not disadvantage the copper coil since the greater sample load is presented to the HTS coil. In spite of these inherent inaccuracies, we present a numerical evaluation of SNR at the center of each coil as an indication of relative performance. For the HTS probe image, the SNR was 17.8 and for the copper probe image, the SNR was 2.4, yielding an advantage of ~7× from using the HTS probe.

Measurements of SNR for the 5-mm HTS probe and the copper Helmholtz pair of similar geometry are shown in Fig. 3. Given the effect of B_1 homogeneity, it is difficult to achieve a 90° pulse at all points in the image. Thus, the transmit power was incremented over a sufficient range to ensure that a 90° excitation was achieved over the greatest fraction of the slice. The high Q coil should transmit power more efficiently, so that a lower power setting is expected to yield a 90° flip angle at a given point. In Fig. 3a, the mean SNR in the image is plotted as a function of transmit attenuation for an RF amplifier with a 100 W maximum output. The maximum SNR can be observed at an attenuation setting of 1 dB for the copper probe, and at a 2.5 dB attenuation setting for the HTS probe. Comparing the ratio of the voltage at these points of peak SNR, and accounting for the effect of pulse time, an increase in efficiency of ~3× is found. In this case, reciprocity of transmitted vs. received voltage does not hold, possibly as a result of current saturation in the HTS coil during transmit (8). Figure 3b shows the images acquired for both coils with the maximum mean SNR. Figure 3c shows histograms of these images. While the maximum signal is uniformly higher in the HTS image, the spread in intensities is also greater, demonstrating the relative increase of RF inhomogeneity in the HTS probe. At the maximum signal point for each coil,

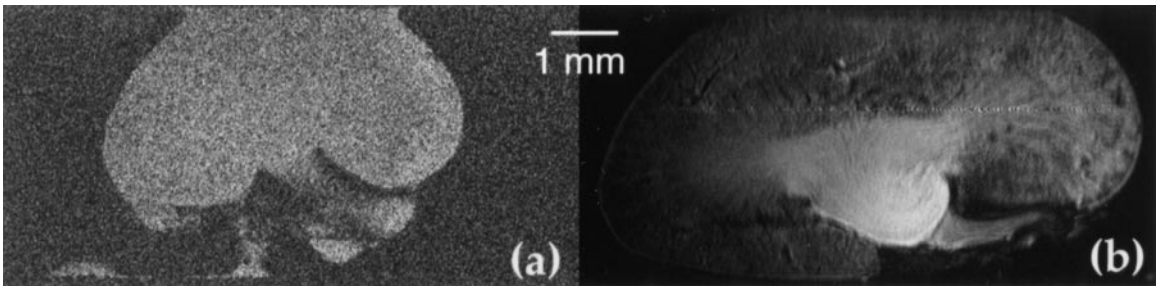

FIG. 2. **a:** 512 × 256 image from a 3D data set of a mouse kidney acquired with the copper Helmholtz probe. In-plane resolution is <20 μm. **b:** Same as a, but taken with the HTS probe.

the SNR gain attained from using the HTS coil was ~7× when comparing both the mean and the maximum SNR values. Although the factor of 7-fold improvement in SNR is substantial; it is less than the 14-fold predicted by the model. The model's ability to provide separate analyses of signal and noise can be demonstrated through further analysis of the sources of this apparent deficit. The predicted signal amplification from the high *Q* coil is a factor of 9.5×, while the projected reduction in the noise floor is a factor of 1.5×. Analyzing signal and noise separately in the images indicates that the entire SNR gain of 7× stems from signal amplification, since negligible reduction in the noise floor is attained. The deficit in signal gain of ~25% is within reason, given that values for inductance and B_1 per unit current are not directly measured. However, the lack of reduction in the noise floor implies that extraneous noise is coupling into the system during imaging. This analysis gives direction to future investigation, since the focus can be narrowed to determining and eliminating these extraneous noise sources.

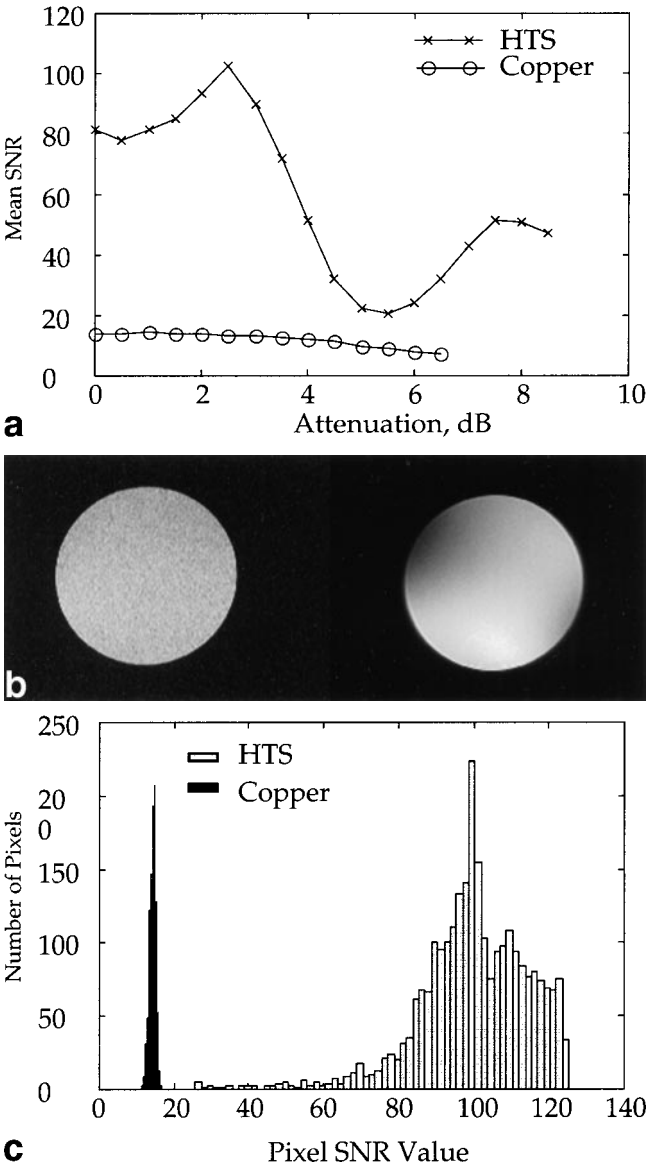

FIG. 3. **a:** Plot of mean SNR as a function of transmit attenuation. **b:** Images from the SNR maxima points in a. Copper image is on the left, HTS image is on the right. **c:** Histogram showing the distribution of the SNR values of the images in b.

RF Homogeneity and Stability

The RF homogeneity of the Helmholtz pair was additionally characterized using axial and sagittal data sets. Profiles of the signal intensity along all three axes of the probe are pictured in Fig. 4. The signals along both the x (Fig. 4a) and y (Fig. 4b) axes of the probe indicate the substantial signal enhancement achieved with the HTS probe. The signal intensity of the HTS coil is less than that of the copper coil in Fig. 4c because of the thinner slice (0.2 vs. 2 mm for the copper coil). Figure 4a demonstrates the homogeneity of the coils along the axis that intersects the center of both coils (y-axis in Fig. 1). While the copper coil pair has a very flat profile on this axis, the HTS probe has a sizable shift in field toward one of the coils in the pair. This shift is possibly the result of the inductance of the tuning loop positioned next to the coil on the left distorting the field lines between the two coils. Figure 4b and c shows the profiles along the horizontal axis of the probe parallel to the two coils and along the vertical axis of the probe, respectively. The homogeneity of the HTS probe along both of these axes is comparable to that of the copper coil pair, with a maximum deviation of 25% between the two coils when comparing normalized intensity values. The degree of homogeneity along these axes indicates the advantage of this design over single-coil HTS probes that suffer from large flip angle variations across the FOV. With exploration of alternate tuning strategies or adiabatic pulses, this probe promises to provide a substantial improvement in homogeneity over prior HTS probe designs along all axes.

The *Q* and resonant frequency as a function of temperature are indicated in Table 2. Even at an operating temperature of 50 K, the *Q* remains above 10,000. The resonant

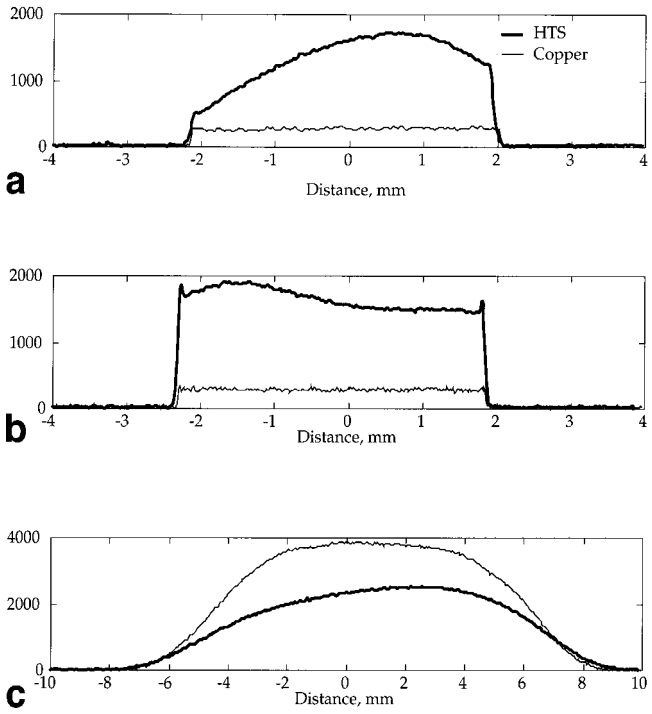

FIG. 4. Plot of signal intensity extracted from image of a water phantom, indicating the homogeneity along all axes of both the copper and HTS probes as described in Fig. 1. **a:** Intensity along y-axis. **b:** Intensity along x-axis. **c:** Intensity along z-axis.

frequency exhibits highly linear behavior over the measured range, with an R^2 value of 0.997. Thus, with the maximum temperature deviation during operation of ± 0.05 K, the corresponding deviation in resonant frequency can be estimated to be approximately 200 Hz, or less than 1% of the coil bandwidth. Some additional frequency drift occurs as the result of thermal contraction and vibration, but is not readily visible in the phantom images.

Comparison With Prior HTS Probes

In light of the operating characteristics documented above, we evaluated the Helmholtz HTS probes in terms of surface coil probes demonstrated by other investigators (3,6–8,21). The largest gains to date were reported by Black et al (7,8) who demonstrated a ~10× gain in SNR when comparing coils of identical geometry. This value is comparable to the 7× gain attained with the Helmholtz HTS probe. If extraneous noise sources are removed so that the effective noise temperature of the Helmholtz HTS coil will be maintained during imaging, the SNR gain will be equal to that reported by Black. This probe has the additional advantage of providing a larger effective FOV through enhanced homogeneity over a single coil design.

Perhaps the most direct comparison can be made between the work presented here and the work presented by Hill (9) for NMR spectroscopy, which demonstrated an SNR gain factor of ~4 over an Alderman-Grant resonator. The diameter of the warm bore for this probe configuration was 5 mm, so that the construction was nearly identical to the HTS microscopy probe introduced here. The difference between the SNR gain achieved in this study and Hill's can mainly be attributed to the difference in filling factor for the comparison coils. The copper coils chosen for this comparison have similar dimensions and field strength per unit current to the HTS coil pair, decoupling the effect of coil geometry from the comparison. Therefore, the substantial SNR gain achieved in this case is mainly a result of the reduced coil resistance in the 5-mm probe.

Table 2
Matched *Q* vs. Temperature

Temperature (K)	Resonant frequency (MHz)	*Q*
15	400.208	19,200
20	400.196	18,700
25	400.185	16,800
30	400.171	16,300
35	400.157	14,700
40	400.139	12,800
45	400.128	12,700
50	400.113	10,100

CONCLUSIONS

A robust NMR microscopy probe with a superconductive volume coil has been constructed and tested, extending earlier work based on surface coils. SNR gains of 7× over a conventional Helmholtz microscopy RF coil were achieved. The operation of this probe under loading conditions typically experienced in our microscopy applications has demonstrated the potential for utilizing this technology to reduce imaging time for a wide variety of high-resolution studies. The specimen shown in Fig. 2 is that of a mouse kidney, which is ~5 mm in diameter. The 17-μm resolution in-plane was achieved in an imaging time of ~1 hr with a mean SNR of ~29. The center frequency of the coil is stable to ~200 Hz (2 pixels) over this imaging period. The practical realization of this volume coil has clearly moved us much closer to the use of HTS technology in enhancing the capabilities of MR microscopy for routine MR histology.

ACKNOWLEDGMENTS

Our gratitude to Elaine Fitzsimons for editing this manuscript and to Gary Cofer for assistance in obtaining the mouse brain images as well as for many helpful discussions. The authors would also like to thank Richard Withers and Robert Nast of Bruker Instruments, as well as Clifford Soble and Bob Black for their contributions to the construction of the superconducting probe. Finally, the authors are grateful to Marielle Delnomdedieu for the preparation of the sample that appears in Fig 2.

REFERENCES

1. Black R, Roemer P, Mueller O. Electronics for a high temperature superconducting receiver system for magnetic resonance microimaging. IEEE Trans BME 1994;41:195–197.
2. Black R, Roemer P, Mogro-Campero A, Turner L, Rohling K. High temperature super-conducting receiver system for magnetic resonance microimaging. Appl Phys Lett 1993;62:771.
3. van Heteren JG, James TW, Bourne LC. Thin-film high temperature superconducting RF coils for low field MRI. Magn Reson Med 1994;32: 396–400.

4. Withers RS, Liang G-C, Cole BF, Johansson M. Thin-film HTS probe coils for magnetic resonance imaging. Trans Appl Superconductivity 1993;3:2450–2453.
5. Miller JR, Zhang K, Ma QY, Mun IK, Jung KJ, Katz J, Face DW, Kountz DJ. Superconducting receiver coils for sodium magnetic resonance imaging. IEEE Trans BME 1996;43:1197–1199.
6. Odoj F, von Kienlin M, Haase A. Cool copper and superconducting coils: the gain in sensitivity for NMR microscopy. In: Proceedings of the International Society for Magnetic Resonance in Medicine, Vancouver, Canada, 1997. p 173.
7. Black RD, Early TA, Roemer PB, Mueller OM, Morgo-Campero A, Turner LG, Johnson GA. A high temperature superconducting receiver for NMR microscopy. Science 1993;259:793–795.
8. Black RD, Early TA, Johnson GA. Performance of a high-temperature superconducting resonator for high-field imaging. J Magn Reson SA 1995;113:74–80.
9. Hill HD. Improved sensitivity of NMR spectroscopy probes by use of high-temperature superconductive detection coils. IEEE Trans Appl Superconductivity 1997;7:3750–3755.
10. Kotsubo V, Nast R. Cryogenic system for a high temperature superconductor NMR probe. Adv Cryogenic Eng 1996;41:1857–1864.
11. Yap M, Black RD, Brey CC, Cole BF, Johansson ME, Johnson GA, Kotsubo VY, Nast R, Wither RS. High temperature superconducting probe for NMR microscopy. In: Proceedings of the Society of Magnetic Resonance 3rd Scientific Meeting. Nice, France, 1995. p 958.
12. Banson MB, Cofer GP, Black RD, Johnson GA. A probe for specimen magnetic resonance microscopy. Invest Radiol 1992;27:157–164.
13. Jerosch-Herold M, Kirschman RK. Potential benefits of a cryogenically cooled NMR probe for room-temperature samples. J Magn Reson 1989;85:141–146.
14. Black RD, Roemer PB, Edelstein WA, Souza SP, Mogro Campero A, Turner LG. Scaling laws and cryogenic probes for NMR microscopy. In ''Proc., 10th Annual Meeting of Society of Magnetic Resonance in Medicine. San Francisco, CA, 1991,'' p. 1250.
15. Hoult DI, Richards RE. The signal to noise ratio of the nuclear magnetic resonance experiment. J Magn Reson 1976;24:71–85.
16. Suddarth S, Fuks F, Black R. Determining preamplifier noise and gain parameters for optimal matching of HTS resonators. In: Proceedings of the SMR 4th Annual Scientific Meeting, New York, 1996. p 1450.
17. Edelstein WA, Bottomley PA, Pfeifer LM. Signal-to-noise calibration procedure for NMR imaging systems. Med Phys 1984;11:180–185.
18. Terman FE. Radio engineers' handbook. New York: McGraw-Hill; 1943.
19. Chen CN, Hoult DI. Biomedical magnetic resonance technology. New York: Adam Hilger; 1989.
20. Hedlund LW, Maronpot RR, Johnson GA, Cofer GP, Mills GI, Wheeler CT. Magnetic resonance microscopy of toxic renal injury induced by bromoethylamine in rats. Fund Appl Toxicol 1991;16:787–797.
21. Hall AS, Alford NM, Button TW, Gilderdale DJ, Gehring KA, Young IR. Use of high temperature superconductor in a receiver coil for magnetic resonance imaging. Magn Reson Med 1991;20:340–343.